Cavity Growth in Underground Coal Gasification Method by Considering Cleat Length and Inclination of Coal with Elasto-Brittle Behavior

Mohammadreza Shahbazi[1], Mehdi Najafi[1*], Mohammad Fatehi Marji[1], and Abolfazl Abdollahipour[2]

1- Department of Mining and Metallurgical Engineering, Yazd University, Yazd, Iran
2- School of Mining Engineering, College of Engineering, University of Tehran, Tehran, Iran

Article Info

Keywords

Abstract

The in-situ coal is converted to the synthetic gas in the process of underground coal gasification (UCG). In order to increase the rate of in-situ coal combustion in the UCG process, the contact surfaces between the steam, heat, and coal fractures should be raised. Therefore, the number of secondary cracks should be increased by raising the heat and existing steam pressure during the process. This paper emphasises on the secondary crack growth mechanism of the pre-existing cracks in the coal samples under different loading conditions. Different geometric specifications such as the length of the pre-existing cracks (coal cleats) and their inclinations are considered. The numerical modeling results elucidate that the first crack growths are the wing cracks (also called the primary or tensile cracks) formed due to unbonding the tensile bonds between the particles in the assembly. Ultimately, these cracks may lead to the cleat coalescences. On the other hand, the secondary or shear cracks in the form of co-planar and oblique cracks may also be produced during the process of crack growth in the assembly. These cracks are formed due to the shear forces induced between the particles as the initial cleat length is increased and exceed the dimension of coal blocks. The cavity growth rate increases as the secondary cracks grow faster in the coal blocks. In order to achieve the optimum conditions, it is also observed that the best inclination angle of the initial coal cleat changes between 30 to 45 degrees with respect to the horizon for the coal samples with the elasto-brittle behavior.

1. Introduction

In the underground coal gasification (UCG) method, coal seams with variable thicknesses are converted to synthetic gas in-situ without traditional mining operations [1]. Recently, research works on UCG has increased, and many modeling research have been done for investigating various effects on the gasification efficiency, flame propagation, coal consumption, etc. [2, 3]. However, this process can cause gas leakage to the surrounding layers, groundwater contamination, surface subsidence, etc., as a result of improper UCG operation, and lead to abnormal evolution of the underground cavity. For the solution of these problems, it is necessary to accurately study the failure behavior of coal and control the process of UCG. In order to

investigate the cavity growth rate and speed in the UCG process, a precise evaluation of the combustion area of the underground coal seam is necessary [4]. Most of the previous research works have examined the cavity growth rates in terms of chemical reactions and operational control of the UCG process [5, 6].

For the safety and productivity of the UCG process, also for evaluating and economizing the UCG method in a coal layer, the rates of both, cavity growth, and coal combustion should be controlled. Accordingly, the evaluation of the cavity growth and environmental hazards need to study the process of cracking or crack propagation in the coal layer under different stress conditions. Therefore, investigating the gas stress resulting

✉ *Corresponding author: mehdinajafi@yazd.ac.ir (M. Najafi).*

from coal combustion at different cavity temperatures and the fracture mechanism of the rocks during and after the UCG process are of the most important operational scenarios to be considered in the UCG method for in-situ coal mining. Although some useful research works have been carried out in the recent years [4, 7], there is little information on the fracture activities including the cracks' initiation and propagation process in the cavity of the UCG method of coal mining. Su *et al*. have performed UCG laboratory simulations on the samples of coal blocks gained from the Kushiro and Bibai Coal Mines in Hokkaido, Japan [4]. They tried to use the in-site UCG models in their laboratory experiments. The results of their studies have shown that increasing the number or size of cracks in the coal layer or coal block, the contact surfaces increase, and the steam and flame resulting from the combustion penetrate into the coal bed via the induced coal surfaces. This phenomenon leads to increase the combustion rate of coal, and increase the cavity growth, and ultimately results in the production enhancement of the synthetic gas. Therefore, the crack initiation and growth increase the cavity growth rate, also raise the calorific value of the gas, which results in the higher quality of the synthetic gas.

It is therefore clear that to analyze the cavity growth rate in the UCG process, it is necessary to examine the parameters affecting the growth of cracks (cleat) in the coal bed.

The fracture mechanics of quasi-brittle or rock-like materials and the mechanism of cracks propagation have been studied in the literature by various researchers for modeling in different numerical solutions [8-12]. Currently, there is a lot of research works on the mechanism of crack propagation in coal at the micro- or macro-scale [13-17]. These research works have been performed using various methods such as the computed tomography (CT) scanning, the scanning electronic microscopy (SEM), the acoustic emission method, the optical microscopy, the high-definition (HD) camerawork, and the numerical simulation methods [4, 18]. Yin *et al*. have performed a CT scan test to investigate the damage evolution in coal under uniaxial compressive load [18]. Zhang and Wong have investigated the initiation, propagation, and coalescence of cracks in quasi-rock materials containing two pre-existing open parallel flaws (stepped and coplanar) under a uniaxial compressive load using a parallel bonded-particle model [19]. They found that wing tensile cracks

were mostly the first cracks to appear in both BPM simulations and physical experiments. Zhao *et al*. have used experimental and numerical methods to investigate the fracturing of coal under impact load [13].

Xie *et al*. have measured the effect of initial crack surface friction on the initiation and propagation of cracks in quasi-rock materials subjected to compressive loads using the extended finite element method (XFEM) [20]. They found that the effect of crack surface friction was the lowest on stress distribution around defects with inclination angles of 30 and 45 degrees. However, as the inclination angle of the defect increased to 60°, the magnitude of this effect increased. Also the starting point and angle of the wing cracks were not affected by friction.

Xiangchun *et al*. have examined the rate of crack propagation in coal containing gas, and have found the relationship between gas pressure and crack propagation rate [14]. Wang *et al*. have studied the mechanical properties of coal masses with cross-sectional cleat networks under uniaxial compressive load [15]. They generated five sets of cubic cleat networks with uniform sizes by using the synthetic rock mass (SRM) method, and finally the effect of uniaxial compressive strength scale (UCS), relationships between fracturing states and strain-stress behaviors and fluctuation main causes in the stress-strain curves were extensively investigated. Wu *et al*. have investigated the crack propagation properties of coal by using three experimental methods, and discussed crack propagation paths and deflection angles [16]. Li *et al*. have performed uniaxial compression tests by using a fracture mechanics model on the coal specimens. During the experiments, a high-quality camera, scanning electronic and optical microscope were used to examine the crack propagation. They have studied the behavior of coal in an underground coal mine with different distances from the coal face [17]. Some research works have been done on the other rock samples; for example, Yue *et al*. have investigated the dynamic fracture coalescence of granite specimens using the Split Hopkinson Pressure Bar system [21]. Lin *et al*. have performed uniaxial compression tests on the jointed rock-like specimens with two dissimilar layers. They investigated the influence of the joint angle and rock bridge angle on the mechanical behavior and failure processes in layered rock masses [22].

The UCG operations are performed underground, and it is not clear exactly where the

coal face is located at each stage of the UCG operation. Therefore, it is necessary to study the growth and propagation of crack to determine the cavity growth and combustion rate from the viewpoint of fracture mechanics in order to have a proper understanding of the coal face condition.

However, the previously reported research on the mechanism of crack propagation in coal is far less than studies on other rock samples. In this study, the cavity growth rate in the UCG process will be investigated by analyzing the production, propagation, and coalescence of primary and secondary cracks under uniaxial compressive loading. In fact, the purpose of this research work is the determine the optimal conditions of the geometric properties of the pre-existing cleat including length and inclination, and its effect on the geo-mechanical parameters to study the cavity growth rate.

2. Crack Propagation Mechanism

The theories of fracture mechanics are used to study the cracks' formation and cracks' growth mechanism in brittle rocks and coals under different loading conditions. However, the crack propagation in the material samples mainly occur due to induced tensile stresses near the pre-existing crack tips [23].

Typically, three types of cracks are propagated in the rock-like materials under compression, as shown in Figure 1 [24]. Primary cracks are formed by the tensile mode of fracture (mode I) at the tip of pre-existing cracks, and two types of secondary cracks (co-planar and oblique) are created by the shear mode (mode II). Thus the wing cracks start from the tip of the flaw due to tensile stresses and propagate along the curved path and eventually align with the loading direction. The secondary cracks resulting from shear stress start at the tip of the defect (initial cleat in coal samples) and propagate parallel or perpendicular to the defect trend. In the elasto-brittle materials, a shear zone is formed around the tip of the pre-existing crack after the growth of the wing crack, and the secondary cracks pass through this shear zone.
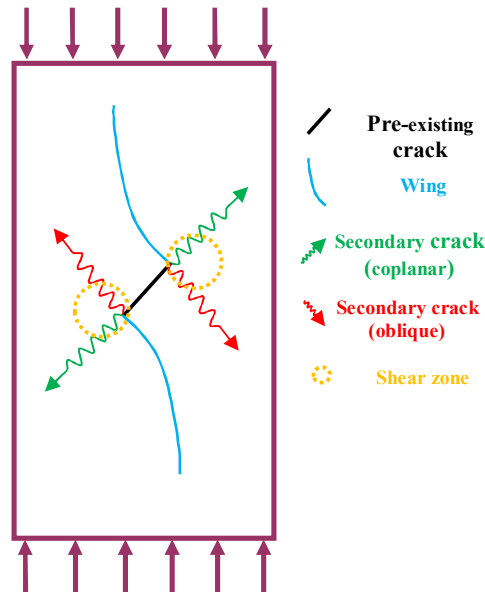

**Figure 1. Pre-existing crack (initiation cleat) grow mechanism due to compressive loading [24].**

The study of crack growth and its propagation mechanism can be performed by the well-established numerical methods in addition to the analytical and semi-empirical methods such as the continuum damage-based models considering the maximum principal tensile strain and F-criterion [25-27]. There are a variety of numerical methods to study the initiating and propagating of cracks with different fracture criteria based on the fracture mechanics' principles such as the finite element method (FEM), discrete element method (DEM), hybrid finite-discrete element methods (FDEM), numerical manifold method (NMM), and displacement discontinuity method (DDM) [24, 27-29].

In this work, a discrete element method is used to accurately predict the crack growing paths and to solve the existing crack extension problems by

adopting a proper crack propagation criterion based on the linear parallel bond model (LPBM). The most important advantage of this method (in the two-dimensional particle flow code (PFC2D)) is that the complex empirical constitutive behavior can be replaced by a simple particle contact logic. The linear parallel bond model can

be arranged in both the ball-ball and ball-facet contacts, as depicted in Figure 2. A parallel bond provides the mechanical behavior of a typical geo-material specimen of cement-like material deposited between the two contacting pieces (ball-ball, or ball-facet) similar to the epoxy cementing the glass beads (Figures 2a and 2b) [30].
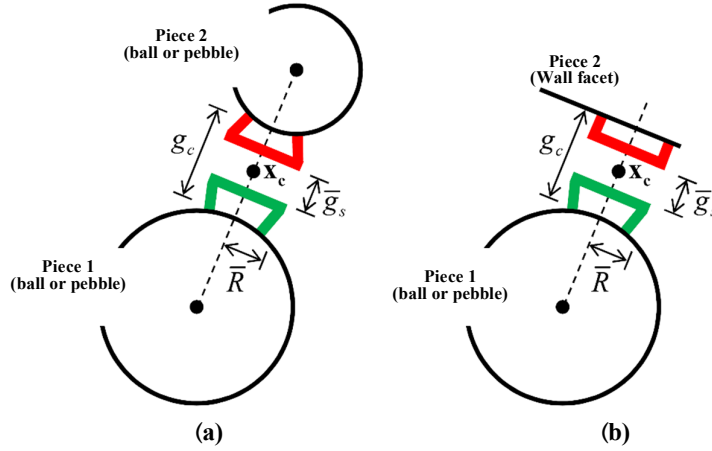
Figure 2. Particle cementation in PFC2D software when parallel bond has not yet been broken considering contact of two particles (a) or contact of one particle with wall facet (b), respectively [30].

Generally, the relationship between particles or pieces and walls is expressed by the force-displacement law in the PFC software. The force-displacement law for the linear parallel bond model, contact force, and the moment is expressed as the following [30]:

$$F_c = F^l + F^d + \overline{F} \tag{1}$$

$$M_c = \overline{M} \tag{2}$$

where F^l, F^d, and $\overline{F}$ are linear force, dashpot force, and the parallel bond force, respectively, and $\overline{M}$ is the parallel bond moment. The parallel bond force is evaluated by a normal and shear force, and the parallel bond moment is evaluated by a twisting and bending moment based on the following equation:

$$\overline{F} = -\overline{F}_n \hat{n}_c + \overline{F}_s \tag{3}$$

$$\overline{M} = \overline{M}_t \hat{n}_c + \overline{M}_b \tag{4}$$

where $\overline{F}_n$ and $\overline{F}_s$ are the normal and shear force from the force, $\overline{M}_t$ and $\overline{M}_b$ are the twisting and bending moment in force-meter, and $\hat{n}_c$ is the normal direction of contact plane, and $\overline{F}_n > 0$ is tension force.

The relationship between the torsional and bending stiffness by torsional and bending moment between particles is defined as follows:

$$M_t = k_t \theta_t, \quad k_t = \frac{GJ}{L} \tag{5}$$

$$M_b = k_b \theta_b, \quad k_b = \frac{EI}{L} \tag{6}$$

where "k_t" and "k_b" are the torsional and bending stiffness, respectively, "θ_t" and "θ_b" are the twist and bend rotation, respectively, "G" is the shear modulus, "J" is the polar moment of inertia of the cross-sectional area about the axis of the shaft, "E" is the Young's modulus, "I" is the moment of inertia of the cross-sectional area about the neutral axis of the beam, and "L" is the length of bond [30].

When a parallel bond is formed through the bond method, an interface is formed between two notional surfaces, and the parallel bond force and moment are equal to zero. A parallel bond creates an elastic corresponding effect between these two notional surfaces, and this interaction is removed as soon as the bond breaks. The relation between maximum normal and shear stress around the parallel bond is expressed as the following equations:

$$\overline{\sigma} = \frac{\overline{F}_n}{\overline{A}} + \beta \frac{\|\overline{M}_b\| \overline{R}}{\overline{I}} \tag{7}$$

$$\bar{\tau} = \frac{\|\overline{F_s}\|}{\overline{A}} + \begin{cases} 0, & 2D \\ \beta \frac{|\overline{M_t}|\overline{R}}{\overline{J}}, & 3D \end{cases} \qquad (8)$$

where $\overline{F}_n$ and $\overline{F}_s$ are the normal and shear forces from the force, $\overline{A}$, $\overline{I}$, and $\overline{J}$ are the cross-sectional area, the moment of inertia, and pole moment of inertia of parallel bond the cross-section, respectively, and $\overline{R}$ is equal to the particle radius, and $\overline{\beta}$ is the moment share ratio and a number between 0 to 1. If the values of the applied normal and shear stress to the bond between particles were more than the above equations, the bond would break and a macro-crack would be formed by linkage of tension, shea, or hybrid micro-cracks [30]. In the following, in order to determine the effect of length and inclination of pre-existing cleat on the crack growth and growth of the cavity, the calibration stages of the sample are expressed.

3. Model Calibration

The PFC calibration is carried out for solving the problem in hand by the linear parallel band model in order to investigate the growth and propagation of cracks in brittle geo-materials by the discrete element modeling techniques.

Therefore, in this research work, 5 bituminous coal samples with elasto-brittle behavior were considered. The values of peak strength, secant elastic modulus, and brittleness for these 5 representative coal samples are shown in Table 1 (a representative sample is a sample that has the average properties of 5 coal samples). The properties of the representative sample are very close to those of the 5 coal samples, and the brittleness indicates the brittle behavior of the samples, as shown in Table 1. Brittleness is area under the stress-strain diagram up to the peak point divided by the total area below the stress-strain diagram (from the beginning to the end of loading) that the closer it is up to 1, the more brittle the material is [31]. The brittleness equation is defined as follows:

$$Brittleness = \frac{AE}{AE + AP} \qquad (9)$$

where "AE" is the area below the strain stress diagram to the peak point and "AP" is the area below the strain stress diagram from the peak point to the end of the loading. Therefore, in this work a representative sample was used for further analysis.

Table 1. Comparison of mechanical properties of 5 coal samples and representative sample used for crack analysis.

Sample	Peak stress (MPa)	Secant modulus of elasticity (GPa)	Brittleness
A	21.14	3.63	0.871
B	17.49	3.99	0.701
C	19.73	2.8	0.775
D	24.49	3.45	0.909
E	25	2.95	0.847
Average of 5 samples	21.57	3.36	0.821
Representative sample	22.53	3.56	0.906

3.1. Calibrating properties of representative sample

In order to calibrate a representative sample, the micro-mechanical and the macro-mechanical properties of the sample must be matched. The conventional tests such as the uniaxial compressive strength (UCS) and the Brazilian tensile strength (BTS) tests are used for this purpose. The investigated samples are cylinders with a diameter and height of 50 mm and 100 mm, respectively. In this calibration procedure, the simulated sample consists of 7244 balls with dimensions of 0.3 mm to 0.6 mm, which are located as constituent particles inside the facets. According to the laboratory sample test, the inter-

grain porosity was equal to 4% and the particle density was equal 1600 kg/m^3. The model s reached initial equilibrium for eliminating the particle overlap and proper emplacement of the particles throughout the simulated sample.

In the linear parallel bonding model, the particles, in addition to the compressive and shear forces, withstand the tensile and bending forces.

In order to simulate the sample behavior consistent with the real laboratory testing specimens, 28 models were built in PFC2D. Therefore, the micro-model parameters must be changed to simulate the macro-behavior. The micro-parameters used for constructing the final numerical model in PFC2D are given in Table 2.

Table 2. Calibrated micro-parameters used for numerical modeling of representative sample.

Micro-parameter	Value	Micro-parameter	Value
emod (GPa)	1.7	g (m)	0.5e-4
Krat	2	Pb_ten (MPa)	7
Rmax (mm)	0.6	Pb_coh (MPa)	6
Rmin (mm)	0.3	Pb_fa (°)	25
ρ (kg/m3)	1600	dp_nratio	0.5

emod: Specify effective young's modulus of the particle	g: Reference gap
Krat : Normal-to-shear stiffness ratio	Pb_ten: Parallel bond tensile strength
Rmax: Upper bound of particle radius	Pb_coh: Parallel bond cohesion
Rmin: Lower bound of particle radius	Pb_fa: Parallel bond friction angle
ρ: Particle density	dp_nratio: Normal critical damping ratio

It should be noted that the Poisson's ratio value is approximately equal to 0.24 using the fish PL (programming language) in the PFC software.

In order to calculate the tensile strength of the simulated sample, the Brazilian test was used. In order to model the sample in the PFC software, a disk with a diameter of 50 mm and a length of 100 mm was subjected to axial loading. The particle radius was between 0.3 mm and 0.6 mm, and 2933 balls or particles were located in a circular container with a diameter of 50 mm.

In this work, the value of force applied at the peak point was approximately 9.184 kN, which concluded that the tensile strength of the sample was 4.67 MPa. Since the tensile strength of the rock was between one tenth and one-fifth of its compressive strength, it follows that the analysis was performed correctly. After calibrating the model and obtaining the micro-mechanical parameters, different lengths and inclination angles of the initial cleat were considered in the model to obtain the best conditions for crack growth in the representative sample because the crack growth pattern had a significant effect on the gasification rate of the in-situ coal in UCG method.

4. Analysis of Results

In general, the cleat networks have a significant impact on the coal strength. It is necessary to study the types of cleats in coal considering the effect of cleat networks on cavity growth in the UCG method. There are generally two main sets of parallel fractures in the coal seam: face cleats and orthogonal butt cleats. Face cleats are formed first, and are oriented perpendicular to the direction of minimum (compressive) principal stress applied on the coal during coalification. Butt cleats form later, and terminate at the face cleats due to the relaxation of the original stress field. As cleats are natural fractures resulting from the interaction of de-volatilization, dehydration and regional tectonics during the coalification process, cleat networks can present with different spatial distributions in the in-situ coal. Field observation and microscopic examination of coal show that the characteristics of total networks are related to the coal type, rank of coal, layer thickness, and regional coal structure [15].

The effect of the parameters such as angle and direction of cleat, cleat step angle, cleat length, length and angle of rock bridge, spacing, and opening on the speed or type of crack growth in coal samples were numerically studied. Figure 3a shows the geometrical view of the expressed and defined parameters. Also Figure 3b shows the distance of a wing crack initiation from the tip of the crack. In the subsequent sections, the angles of the wing crack, co-planar and oblique cracks initiated relative to the applied vertical stress were calculated. Therefore, in this work, the geometric effects of cleat (or natural fractures) were examined considering different lengths and angles (0 to 90 degrees relative to the horizon) away from the coal face that are not affected by the high heat, the synthetic gas pressure, and the stress induced due to coal caving.
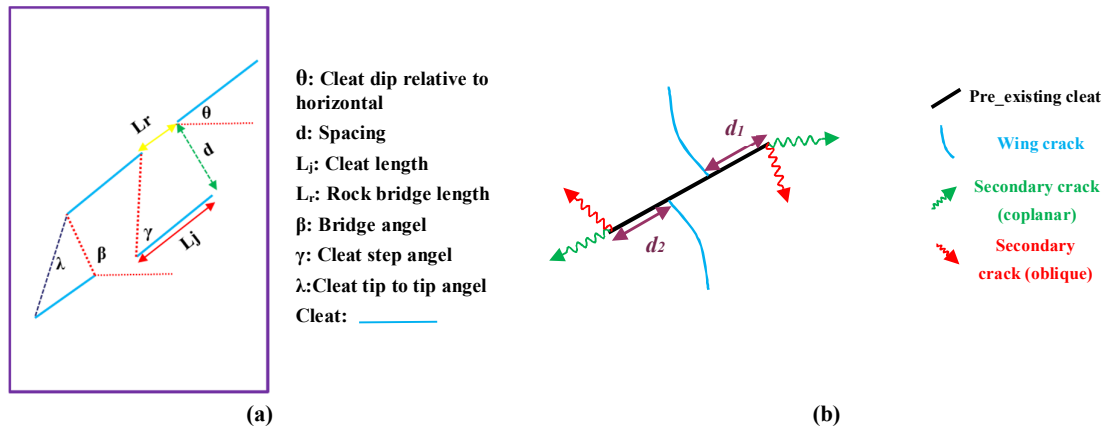
Figure 3. Characteristics of primary cleat and secondary cracks a: Geometric parameters to investigate effect of geometric properties of cleat on crack growth in coal, b: Characteristics of distance wing crack tip from primary cleat tip.

Two geometric parameters were examined for the pre-existing flaws (cleats) in the coal sample (i.e. the length and inclination angle of the cleat) in such a way as to obtain the best conditions for the crack growth pattern. The geometric parameters of the length and inclination angle of the coal cleat are shown in Table 3. Also the effects of these parameters were investigated on the model output that included the length and angle of the wing crack, type of the propagated crack, peak stress, strain at the peak stress, crack initiation stress, distance from the crack tip, shear crack length, number of micro-cracks at the peak stress, brittleness, and the elastic modulus.

Table 3. Investigation of changes in different parameters of coal cleat on crack propagation in representative sample.

Mode	1	2	3	4	5	6	7
Cleat length to sample width ratio	0	0.08	0.1	0.2	0.3	0.4	0.5
Dip (°)	0	15	30	45	60	75	90

In the following section, the effects of cleat length to sample width ratio and cleat inclination angle on the crack growth mechanism and geo-mechanical parameters for the cavity growth in a coal bed are investigated.

4.1. Effects of sample geometry such as e ratio of cleat length to sample width on its mechanical behavior

Changes in the cleat length to the width of the sample (50 mm) were done according to the ratios expressed in Table 3. Figures 4 and 5 show the changes in the cleat length parameter on other geo-mechanical parameters that these diagrams can help to analyze and interpret the effect of the initial cleat on the growth of secondary cracks and failure of the coal sample.
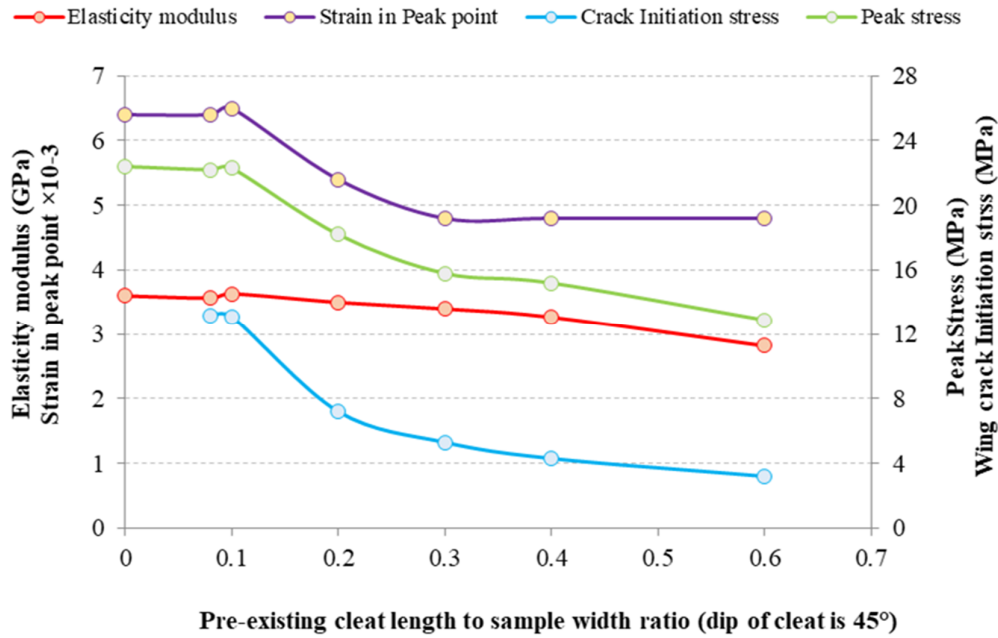
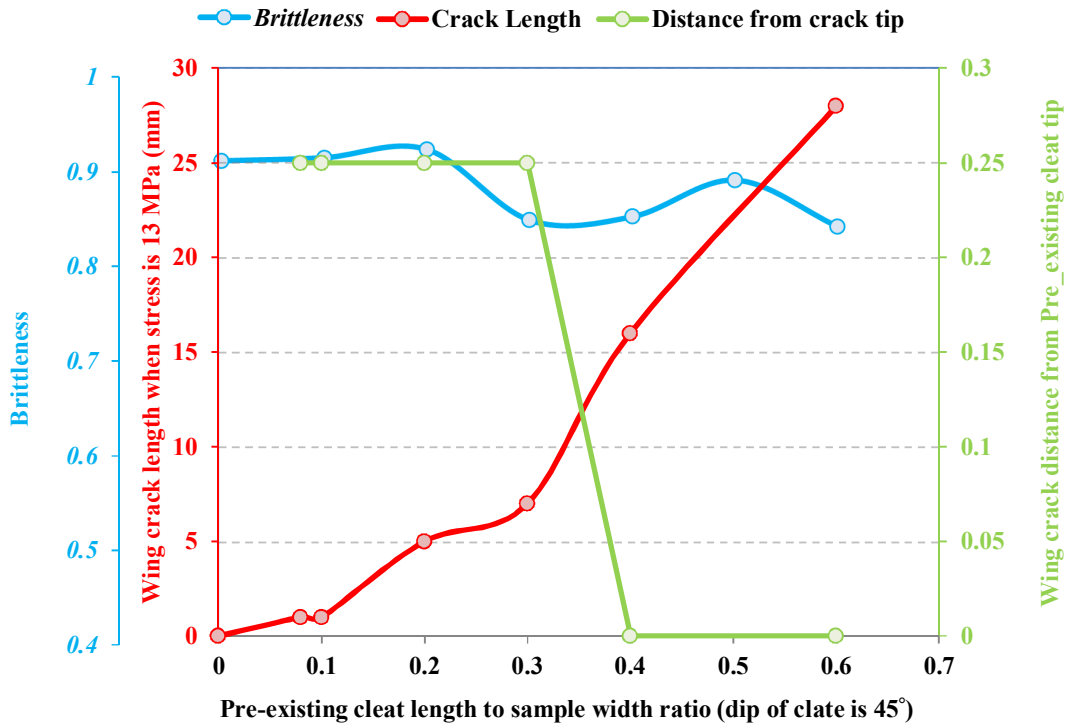**Figure 4. Effect of cleat length on geo-mechanical parameters.**

Figure 5. Effect of coal cleat length on wing crack length, distance of new crack formation from crack tip and brittleness

The modulus of elasticity and the value of strain at the peak stress decrease with increasing the cleat length, as shown in Figure 4, so that by increasing the cleat length relative to the sample width to 0.6 is encountered by decreasing 21 and 25 percent compared to the initial state, respectively. Also the value of peak stress and crack initiation stress in the maximum value of

cleat length is reduced by 42% and 75%, respectively, compared to the state of intact coal sample (without cleat). This value indicates a decrease in the elastic state of the specimen and a move towards the plastic behavior, and as the cleat length increases, the specimen fracture will occur with less load and more easily than the specimen without the cleat.

Also brittleness and the average distance between the right and left side wing crack formation of the crack tip decreases with increasing cleat length. The increase value of wing crack length was investigated in different values of cleat length at applied stress (13 MPa), which showed that the length of wing tensile crack increased by increasing cleat length. The created wing crack angle with relative to the applied vertical stress in the counterclockwise does not show a definite trend, and its so-called values are sinusoidally and alternately increasing and decreasing. Also co-planar and oblique cracks do not form in all samples. The co-planar cracks are formed in the ratio of cleat length to sample width with values of 0.2, 0.3, and 0.6, and its

angle respect to the vertical stress applied in the counterclockwise increases in these three samples with increasing cleat length. Oblique cracks are formed in the ratio of cleat length to sample width with values of 0.2, 0.4, and 0.6, and its angle respect to the vertical stress applied in the counterclockwise is not a specific trend in these three samples.

Figure 6 shows the total of the created cracks and the strain-stress diagram in samples with different cleat lengths. According to this figure, with increasing the cleat length, the value of peak strength and elastic behavior of the sample decreases, and the number of micro-cracks increases. The number of tensile or shear micro-cracks at first increases and then decreases in all 6 samples at the peak strength point of the stress-strain diagram with increasing the length of the initial cleat, and generally shows an increase of 8% to 160% compared to the sample without cleat. At the end of loading, the number of micro-cracks in the sample with the longest cleat has the highest value.
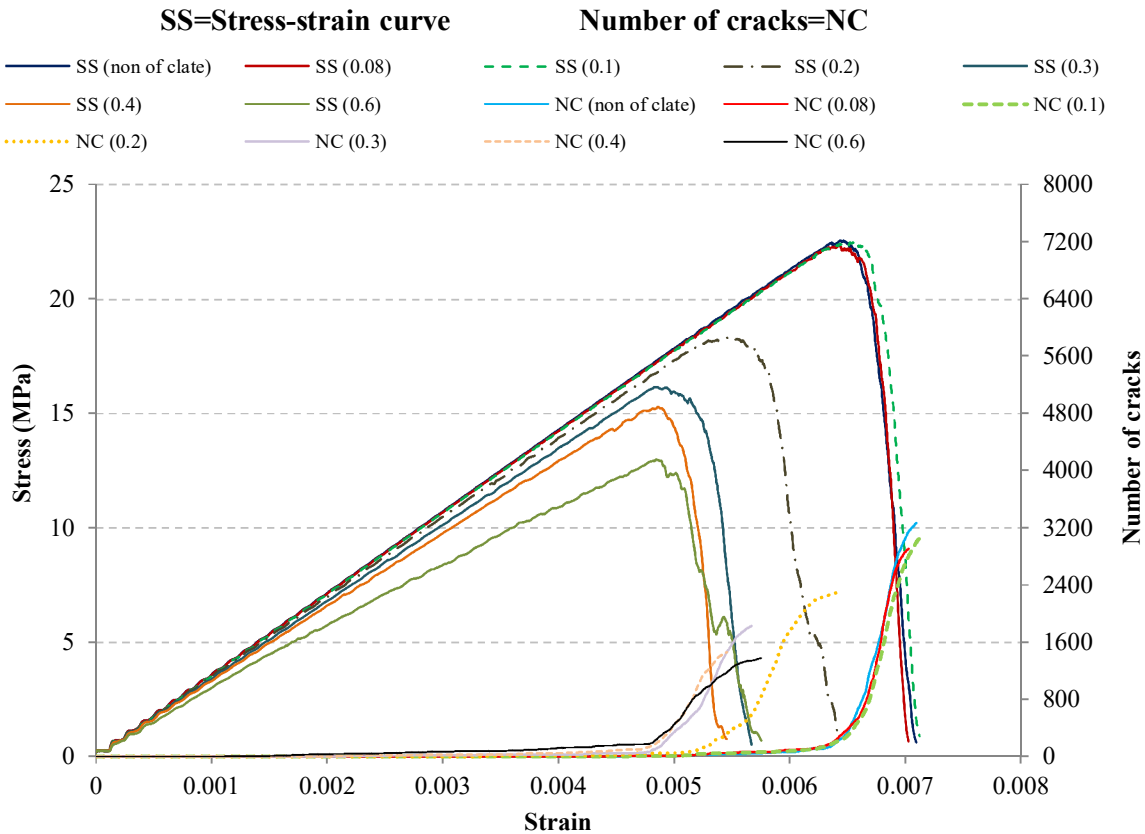

Figure 6. Number of created micro-cracks and strain-stress diagram of coal sample with different initial cleat lengths (cleat length inside parentheses is shown in mm).

The value of the required force to break the normal and shear bond in the wing crack path relative to the increase in cleat length is shown in Figures 7 and 8. In these figures, the values of normal and shear force for breaking the bond are shown at three points near the tip of the crack, the middle point and the end point of the wing crack (monitored points). The monitored points in the crack path are defined so that the parameters are measured at these points, as are shown in Figure 9.

As it is known, the maximum value of normal and shear required force to break the bond is the case that the ratio of cleat length to the width of the sample is 0.1, and by increasing this ratio, the value of the required force decreases to break the bond. Also the value of normal force for bond

break is always greater than the shear force. Therefore, in the UCG method with brittle geo-elastic behavior, if the coal blocks are formed in such a way that the cleat dimensions to the block are equal to 0.1, cavity growth will be slower. Moreover, in these diagrams the values of the formed wing crack angle respect to applied vertical stress and the length of the wing crack relative to the cleat length was shown. As the cleat length increases, the wing crack length increases at a certain stress, and the wing crack angle does not show a definite trend. Also the initiation stress of co-planar and oblique cracks decreases with increasing cleat length of coal. It should be noted that this type of crack is not formed in all samples.

Monitored points for force required to break normal force contact (bar chart)
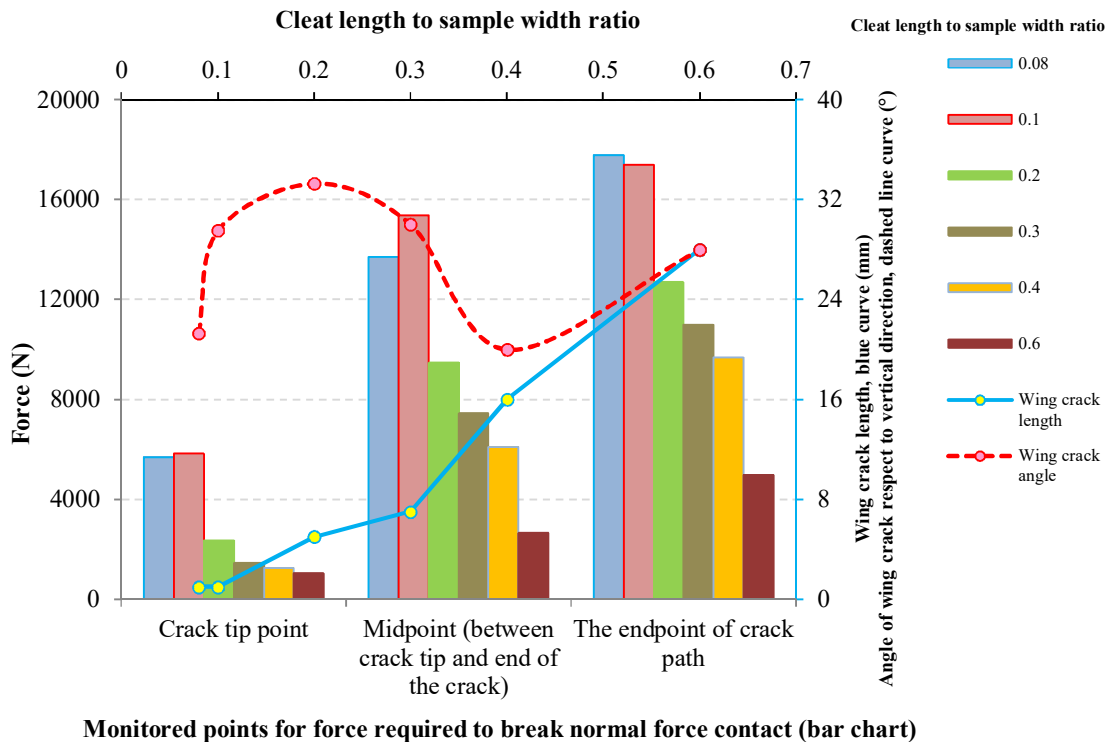
Figure 7. Value of normal required force to break parallel bond between particles and changes in length and wing crack angle relative to changes in cleat length.

4.2. Changes in coal cleat inclination angle

The cleat of coal can have inclination due to the existing tectonic conditions, different stresses resulting from the cavity roof caving in the UCG method and the different sequences of coal seams. For this purpose, the effect of cleat inclination on crack growth was done in the representative coal

sample (in Table 1), which has elasto-brittle behavior, and it can be said that the inclination parameter plays an important role in changes in the crack propagation length, direction, and velocity. For this work, the considered cleat inclinations were 0, 15, 30, 45, 60, 75, and 90 degrees relative to the horizon.

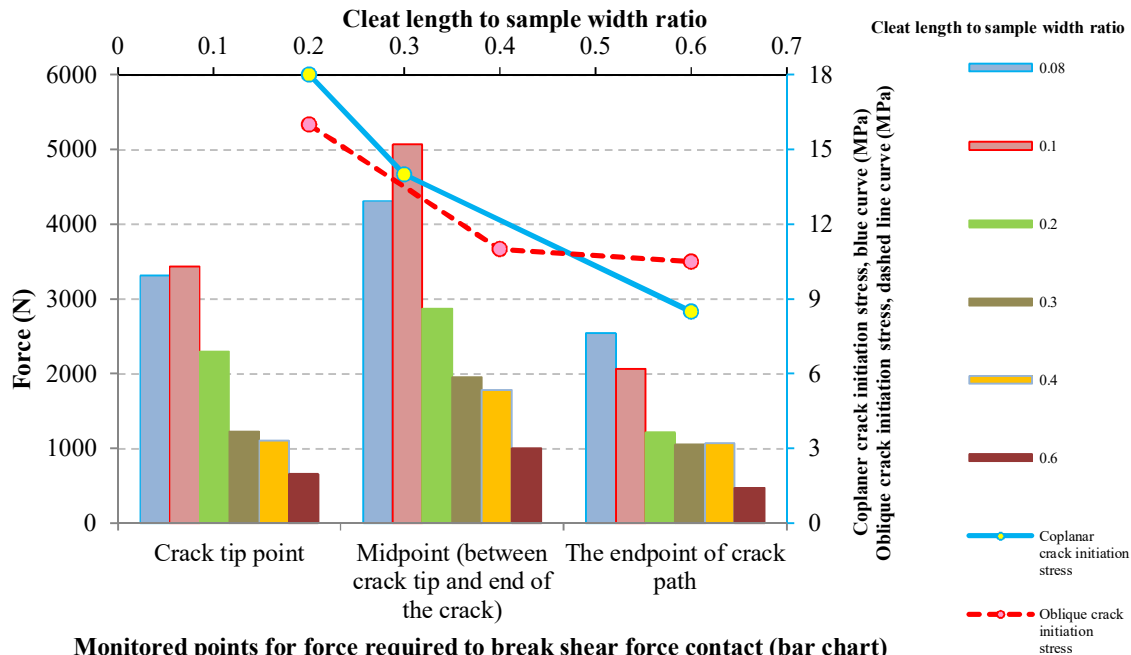**Monitored points for force required to break shear force contact (bar chart)**

Figure 8. Value of shear required force to break parallel bond between particles and changes in and co-planar and oblique cracks initiation stress respect to changes in cleat length.
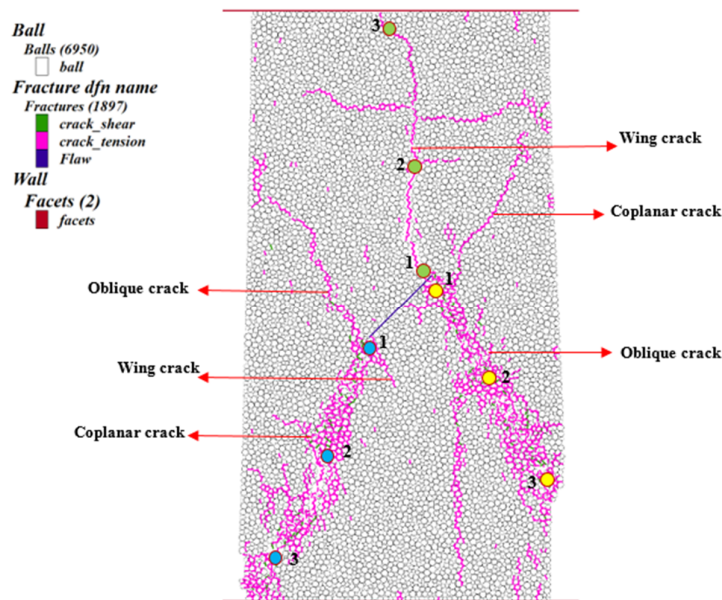

Figure 9. Monitored points located in the path of various types of cracks.

The cleat length in all samples was considered to be 15 mm, and the effect of inclination changes on the output of the analysis parameters is shown in Figures 10 and 11. The value of peak strength and strain (in peak strength) decreases with increasing the inclination of the initial cleat in the sample from 0 to 45 degrees and increases from an inclination of 45 degrees, as shown in Figure 10. The value of this increase is done with more rate after 45 degrees for cleat inclination. This

condition also occur for the wing crack initiation stress, i.e. it has a decreasing trend up to a 45 degree (for cleat inclination) and then an increasing one. The modulus of elasticity affectivity is negligible against these changes. The crack initiation stress in the cleat with an angle of 45 degrees is about 40% and 66% less than the initial horizontal and vertical cleat state, respectively. The value of peak strength in cleat with a 45 degree angle is 30% less than the peak

strength in the sample without initial cleat.

The value of wing crack length (when stress is 15 MPa) has an increase-decrease trend relative to initial cleat inclination increasing, i.e. it reaches its value maximum up to an inclination of 30 degrees of cleat, which is about 3.3 times its value in the cleat inclination of 60 degrees, and after this decreases. Wing cracks are not formed in the cleat inclination of 75 and 90 degrees, and the specimen is ruptured in shear (diagonally). The distance of wing crack formation decreases from the pre-existing crack (cleat) tip of coal with increasing cleat inclination, which has also happened in the previous studies on various rocks with brittle behavior. The brittleness value increases with increasing the inclination of the initial cleat so that in the inclination of the initial cleat of 90 degrees the brittleness value is 20% more than the case where the initial cleat is horizontal. The brittleness value with a cleat inclination of 90 degrees relative to the horizon is equal to a sample that lacks the initial cleat.
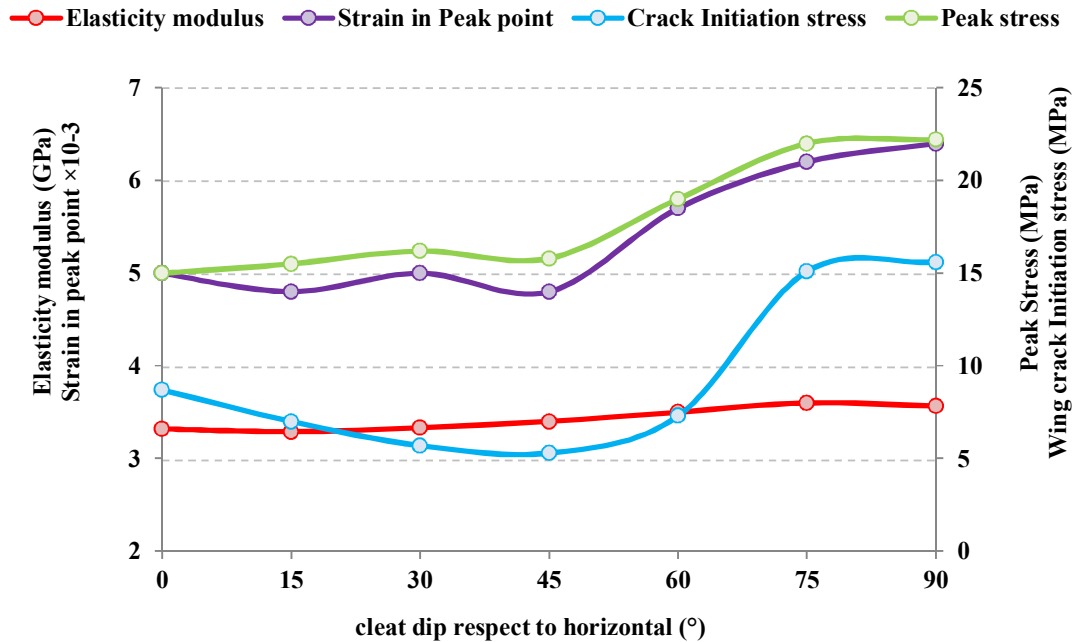
Figure 10. Effect of cleat inclination angle on geo-mechanical parameters of coal sample.

The normal force of the crack tip required to break the bond between the particles in terms of cleat inclination changes is shown in Figure 12. According to this figure, it is clear that with increasing the cleat dip, the amount of required force to break the bond increases. The value of this force is the lowest at the crack (cleat) tip. This parameter is inverse relation to the value of wing crack length, i.e. with more bond force between the particles, the wing crack length decreases, which seems quite reasonable. The maximum length of wing crack length is formed in the cleat inclination of 0 and 30 degrees. This work was performed up to a cleat inclination of 60 degrees relative to the horizon because at a cleat inclination of 75- and 90-degrees wing cracks were not formed in the sample. As the cleat inclination increases, the wing crack angle also increases because with the rotation of the cleat in different samples in a counterclockwise direction, the formed wing cracks also repeat this process so that its angle with respect to the horizon increases.
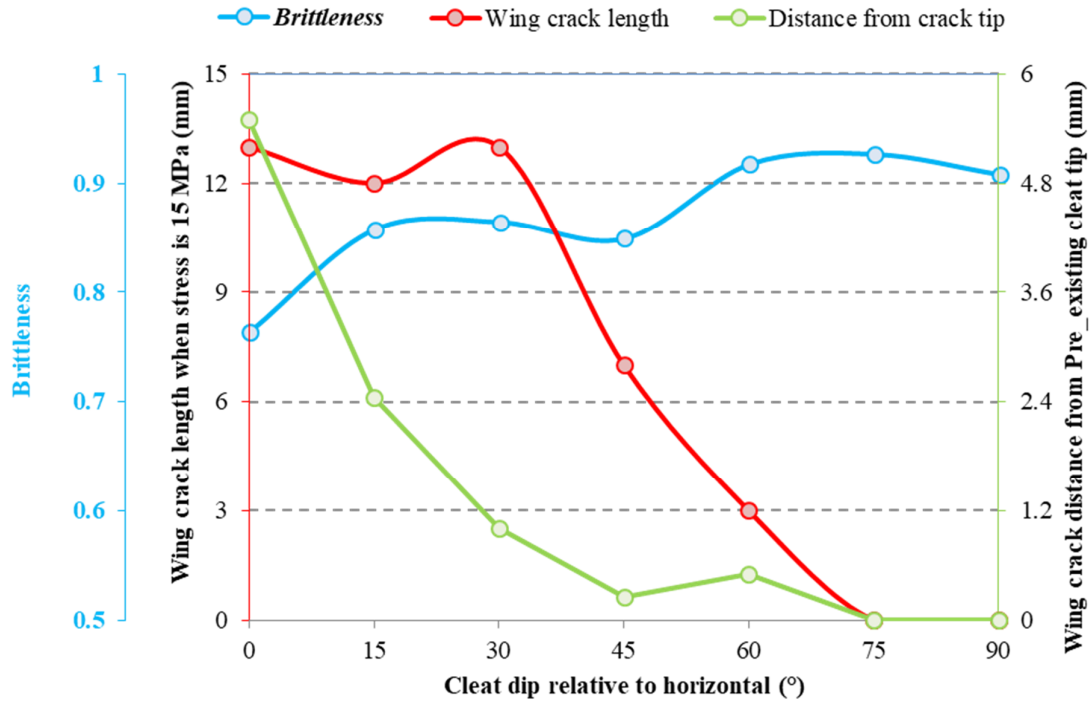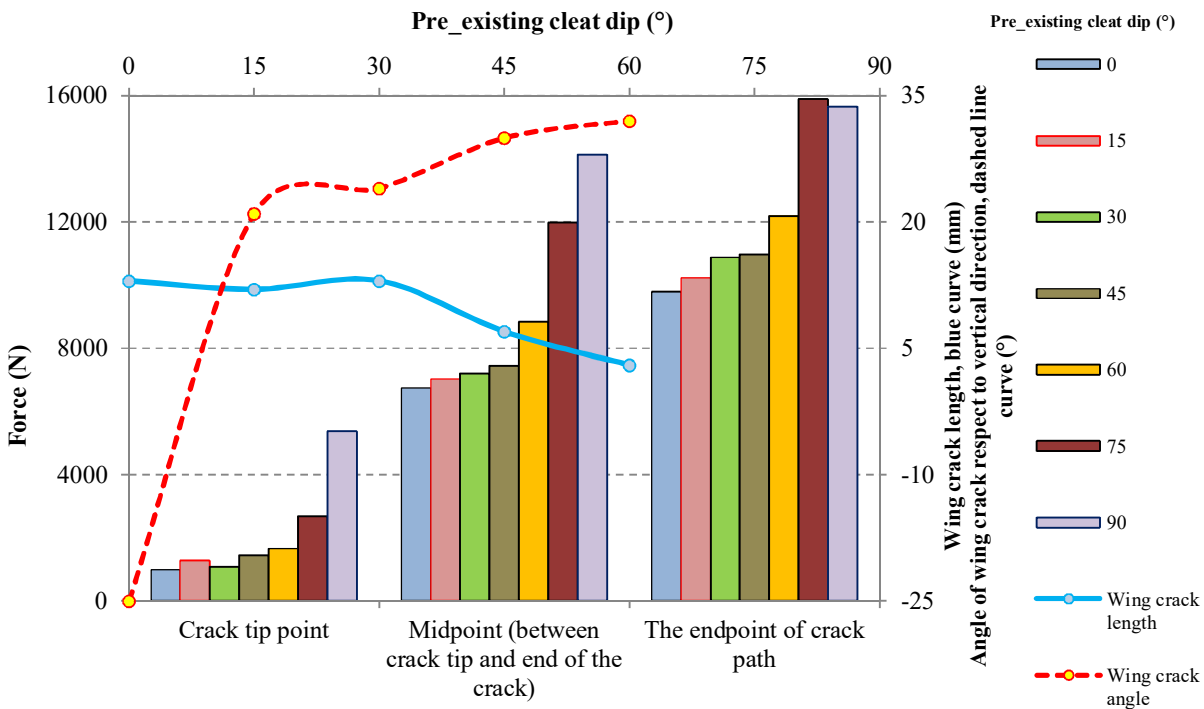
Figure 11. Effect of cleat inclination angle on length of wing crack, distance of new crack formation from crack tip, and brittleness of coal sample.


Figure 12. Value of normal force required to break parallel bond between particles and changes length and angle of wing crack relative to changes in inclination angle of coal cleat.

It should be noted that the shear force changes required to break the bond between the particles relative to cleat inclination are similar to the normal force and are not expressed. Also oblique and co-planar cracks cannot be examined due to the lack of formation in some samples and their oscillating changes, and they do not have a specific trend. Figure 13 shows the sum of the cracks created and the strain-stress diagram in samples with different cleat inclination. According to this figure, the value of peak strength decreases by increasing the cleat inclination up to an angle of 45 degrees, and then

increases so that it reaches its maximum value at an angle of 90 degrees. The value of the peak strength with a cleat inclination of 90 degrees is equal to the state that the sample does not have initial crack or the cleat. The elastic behavior of the sample increases negligibly up to a cleat inclination of 75 degrees, and the number of created micro-cracks doubles up to a cleat inclination of 60° and after that decreases. On the whole, the number of micro-cracks shows increasing between 3% to 211% compared to the sample without cleat.
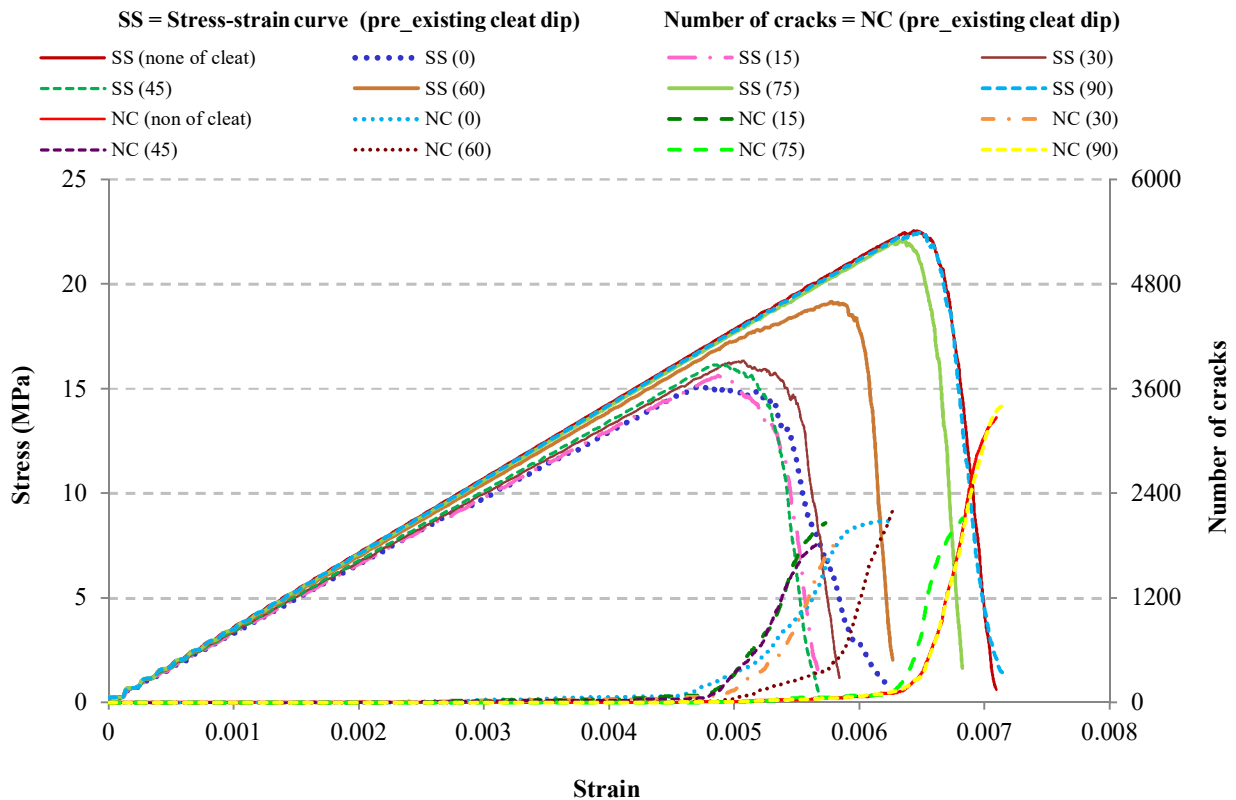
Figure 13. Number of created micro-cracks and samples' stress-strain diagrams with different initial cleats' inclination angles (shown in parentheses and in degrees).

According to the above, the lowest peak stress and crack initiation stress are formed in a sample with a cleat inclination of 45 degrees relative to the horizon. On the other hand, the most growth occurs in wing crack in the sample with the initial cleat with an inclination of 30 degrees compared to other samples. Since connection and coalesce of pre-existing cracks is done in the UCG process with wing cracks (because the wing cracks are the first cracks to form), so the best angle of

inclination of the initial cleat can be between 30 and 45 degrees relative to the horizon for bituminous coal with brittle behavior (elasto-brittle) in order to maximize the cavity growth rate. Table 4 shows the tensile and shear crack propagation and particles fragment condition of all samples at the end of loading considering the types of length and inclination of the simulated initial cleat in this study.

Table 4. Effect of initial size and inclination cleat on crack propagation and particles fragment condition of samples at end of loading.
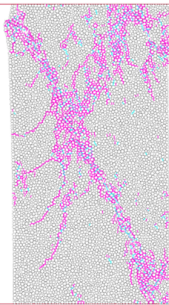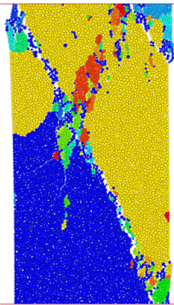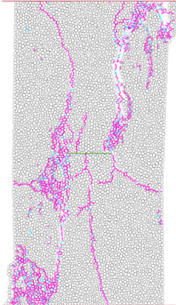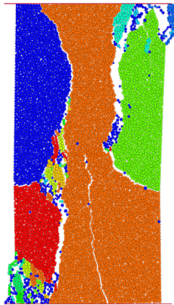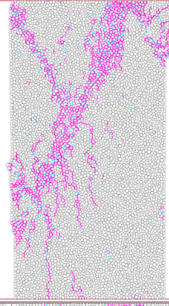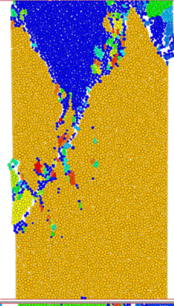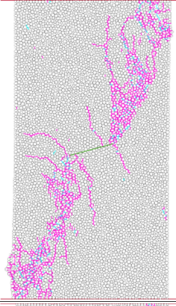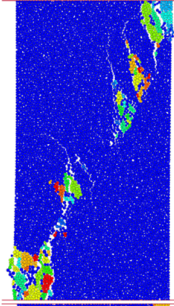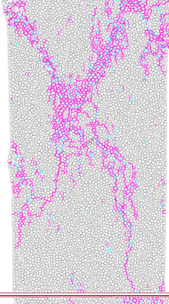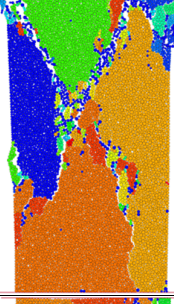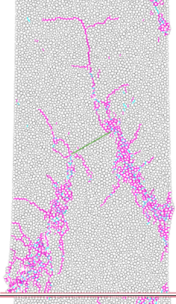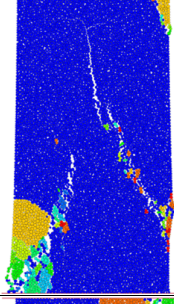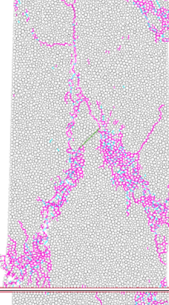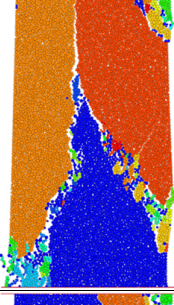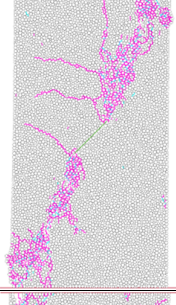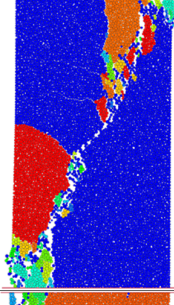
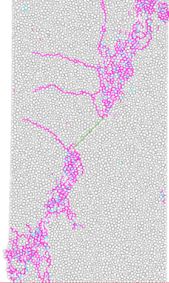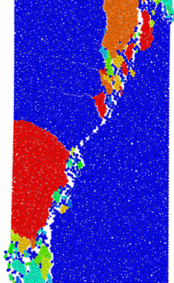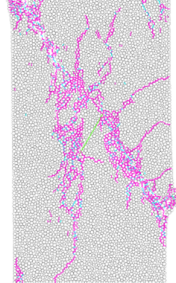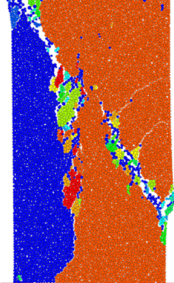| Cleat length	Crack propagation	Sample fragment	Cleat dip	Crack propagation	Sample fragment	Legend
None of pre-existing — **0**			**0**			*Fracture dfn name* — *crack_shear* / *crack_tension* / *Pre-existing cleat* ; *Ball fragment Balls (7244)* : 1.3400E+02, 1.3000E+02, 1.2000E+02, 1.1000E+02, 1.0000E+02, 9.0000E+01, 8.0000E+01, 7.0000E+01, 6.0000E+01, 5.0000E+01, 4.0000E+01, 3.0000E+01, 2.0000E+01, 1.0000E+01, 0.0000E+00
Pre_existing Cleat length to sample width ratio — **0.1**			**15**			
0.2			**30**			
0.3			**45**			
0.4			**60**			

Pre-existing cleat inclination respect to horizontal (°)

Table 4. Continuous of Table 4.

s		75	
0.5		90	

5. Conclusions

In this work, the effects of geometrical parameters of the initial cleats in coal samples were considered to investigate the cavity growth rate in the UCG process by the particle flow code in two dimensions (PFC2D), which is a numerical software based on the versatile discrete element method (DEM). A discrete element method called the linear parallel bond model was used to accurately investigate the crack path and the type of formed cracks in the coal samples. The most important reason for using this method is that it is suitable for investigating the path and dimensions of shear cracks, which are easily distinguishable from the micro-tensile cracks. In this research work, the crack propagation mechanism of brittle coal was investigated considering an elasto-brittle behavior for coal, which was followed by the cavity growth in the UCG process of in-situ coal mining. The changes in the cleat length and its inclination angle in coal samples were studied to investigate the crack propagation pattern and the of the cavity growth of the coal seam on the length and angle of the wing cracks, type of the propagated cracks, peak stress, value of the strain at peak stress, crack initiation stress, distance from the crack tip, shear crack length, number of micro-cracks at the peak stress, brittleness, and the modulus of elasticity of the representative coal sample.

The most important results of this research work are as follow:

- A shear zone is formed in the coal sample with brittle behavior. This is a high strength zone around the tip of the pre-existing cleat, where the secondary oblique and co-planar cracks are being produced after the growth of wing cracks and pass through this shear zone.

- The average normal forces required to break the bonds in the assembly for the wing cracks are less than those for oblique and coplanar cracks so that the growth of tensile wing cracks occurs faster than the shear in the coal sample.

- The modulus of elasticity and the value of strain at the peak stress decrease with increasing the cleat length, as the cleat length increases, the specimen fracture will occur with less load and more easily than the specimen without the cleat. Also brittleness decreases and the length of wing tensile crack increases by increasing the cleat length. With increasing the cleat length, the value of peak strength and elastic behavior of the sample decreases and the number of micro-cracks increases.

- The value of peak strength and strain (in peak strength) decreases with increasing the inclination of the initial cleat in the sample from 0 to 45 degrees, and increases from an inclination of 45 degrees. This condition is also occurring for the wing crack initiation stress, i.e. it has a decreasing trend up to a 45 degree (for cleat inclination) and then an increasing one. The lowest peak stress and crack initiation stress are formed in a sample with a cleat inclination of 45 degrees relative to the horizon. This condition also occurs for the wing crack initiation stress, i.e. it has a decreasing trend up

to a 45 degree (for cleat inclination) and then an increasing one. The modulus of elasticity affectivity is negligible against these changes. Generally, the length of the wing crack decreases and the brittleness increases by increasing the inclination of the initial cleat.

- According to the modeling of this research work, it is concluded that in the underground coal gasification method with brittle geo-elastic coal behavior, the coal blocks are formed in such a way that the dimensions of the initial cleats relative to that of the coal block are considerable so that the cavity growth rate occur faster and increasing the production rate of the synthetic gas. Also the best initial cleat inclination angles can be between 30 and 45 degrees with respect to the horizon for bituminous coal with brittle (elasto-brittle) behavior in order to maximize the cavity growth rate due to the lowest peak and crack initiation stresses which ultimately leads to the maximum growth rate of the wing cracks in the coal samples.

Declaration related to conflict of interests

The authors declare that there is no conflict of interest.

Availability of data and material

All data and models generated or used during the study appear in the submitted article.

Funding

Acknowledgment

References

[1]. Couch, G.R. (2009). Underground Coal Gasification. London, UK: IEA Clean Coal Centre.

[2]. Saulov, D.N., Ovid, A.P. and Klimenko, A.Y. (2010). Flame propagation in a gasification channel. Energy, 35, 1264–73.

[3]. Blinderman, M.S., Saulov, D.N., and Klimenko, A.Y. (2008). Forward and reverse combustion linking in underground coal gasification. Energy. 33 (3): 446-454.

[4]. Su, F., Itakura, K., Deguchi, G. and Ohga, K. (2016). Monitoring of coal fracturing in underground coal gasification by acoustic emission techniques. Applied Energy, 189, 142-156.

[5]. Javed, S.B., Uppal, A.A., Bhatti, A.I., and Samar, R. (2019). Prediction and parametric analysis of cavity growth for the underground coal gasification project Thar. Energy, 172, 1277-1290.

[6]. Gao, W., Zagorscak, R. and Thomas, H, R. (2021). Insights into solid-gas conversion and cavity growth during Underground Coal Gasification (UCG) through Thermo-Hydraulic-Chemical (THC) modelling. International Journal of Coal Geology, 237, 103711.

[7]. Shahbazi, M., Najafi, M. and Marji, M.F. (2018). On the mitigating environmental aspects of a vertical well in underground coal gasification method, Mitigation and Adaptation Strategies for Global Change, 24, 373–398.

[8]. Marji, M.F. (1997). Modelling of cracks in rock fragmentation with a higher order displacement discontinuity method. PhD Thesis in Mining Engineering (Rock Mechanics), METU, Ankara, Turkey.

[9]. Haeri, H., Sarfarazi, V., Ebneabbasi, P., Shahbazian, A. and Marji, M.F. (2020). XFEM and experimental simulation of failure mechanism of non-persistent joints in mortar under compression. Construction and Building Materials, 236, 117500.

[10]. Haeri, H., Sarfarazi, V., Zhu, Z., Marji, M.F. and Masoumi, A. (2019). Investigation of shear behavior of soil-concrete interface. Smart Structures and Systems. 23 (1): 81-90.

[11]. Haeri, H., Khaloo, A.R., Shahriar, K., Marji, M.F. and Moaref Vand, P. (2015). A boundary element analysis of crack-propagation mechanism of micro-cracks in rock-like specimens under a uniform normal tension. Journal of Mining and Environment. 6 (1): 73-93.

[12]. Sarfarazi, V., Haeri, H., Marji, M.F. and Zhu, Z. (2017). Fracture mechanism of Brazilian discs with multiple parallel notches using PFC2D. Periodica Polytechnica Civil Engineering. 61 (4): 653-66.

[13]. Zhao, Y.X., Zhao, G.F. and Jiang, Y.D. (2013). Experimental and numerical modelling investigation on fracturing in coal under impact loads. International Journal of Fracture, 183, 63–80.

[14]. Xiangchun, L., Chao, W., Caihong, Z. and Hua, Y. (2012). The propagation speed of the cracks in coal body containing gas. Safety Science. 50 (4): 914-917.

[15]. Wang, C., Zhang, C., Li, T. and Zheng, C. (2019). Numerical investigation of the mechanical properties of coal masses with T-junctions cleat networks under uniaxial compression. International Journal of Coal Geology, 202, 128-146.

[16]. Wu, P.F., Liang, W.G., Li, Z.G., Cao, M.T. and Yang, J.F. (2016). Investigations on mechanical properties and crack propagation characteristics of coal and sandy mudstone using three experimental methods. Rock Mechanics and Rock Engineering, 50, 215-223.

[17]. Li, L., Yan, S., Liu, Q. and Yu, L. (2018). Micro- and macroscopic study of crack propagation in coal: theoretical and experimental results and engineering practice. Journal of Geophysics and Engineering. 15 (4): 1706-1718.

[18]. Yin, G.Z., Gao, D.F. and Pi, W.L. (2003). CT real-time analysis of damage evolution of coal under uniaxial compression. J. Chongqing Univ, 26, 96–100.

[19]. Zhang, X.P. and Wong, L.N.Y. (2012). Crack Initiation, Propagation and Coalescence in Rock-Like Material Containing Two Flaws: A Numerical Study Based on Bonded-Particle Model Approach. Rock Mechanics and Rock Engineering, 46,1001–1021.

[20]. Xie, Y., Cao, P., Liu, J. and Dong, L. (2016). Influence of crack surface friction on crack initiation and propagation: A numerical investigation based on extended finite element method. Computers and Geotechnics, 74, 1-14.

[21]. Yue, Z., Peng, L., Yue, X., Wang, J. and Lu C., (2020). Experimental study on the dynamic coalescence of two-crack granite specimens under high loading rate. Engineering Fracture Mechanics 237, 107254.

[22]. Lin, Q., Cao, P., Wen, G., Meng, J., Cao, R. and Zhao, Z. (2021). Crack coalescence in rock-like specimens with two dissimilar layers and pre-existing double parallel joints under uniaxial compression. International Journal of Rock Mechanics & Mining Sciences, 139, 104621.

[23]. Sharafisafa, M. and Nazem, M. (2014). Application of the distinct element method and the extended finite element method in modelling cracks and coalescence in brittle materials. Computational Materials Science, 91, 102–121.

[24]. Marji, F.M. (2014). Numerical analysis of quasi-static crack branching in brittle solids by a modified displacement discontinuity method. International Journal of Solids and Structures. 51 (9): 1716-1736.

[25]. Reyes, O. and Einstein, H.H. (1991). Failure mechanism of fractured rock—a fracture coalescence model. Proceedings of the seventh international congress on rock mechanics, Aachen, Germany.

[26]. Vaughan, H. (1998). Crack propagation and the principle-tensile-stress criterion for mixed-mode loading. Engineering Fracture Mechanics. 59 (3): 393-397.

[27]. Shen, B. and Stephansson, O. (1994). Modification of the G-criterion for crack propagation subjected to compression. Engineering Fracture Mechanics. 47 (2): 177–189.

[28]. Bakhshi, E., Rasouli, V., Ghorbani, A., Marji, F.M., Damjanac, B. and Wan, X. (2019), Lattice Numerical Simulations of Lab-Scale Hydraulic Fracture and Natural Interface Interaction, Rock Mechanics and Rock Engineering. 52 (5): 1315-1337.

[29]. Lak, M., Marji, F.M., Bafghi, A.Y. and abollahipour, A. (2018). Discrete element modeling of explosion-induced fracture extension in jointed rock masses. Journal of Mining and Environment. 10 (1): 125-138.

[30]. Itasca consulting group, Inc. PFC 2D Version 6.00. (www.itascacg.com).

[31]. Zhang, B., Bicanic, N., Pearce, C.J. and Phillips, D.V. (2002). Relationship between brittleness and moisture loss of concrete exposed to high temperatures. Cement and Concrete Research, 32, 363-371.

گسترش فضای استخراجی در روش گاز کردن زیرزمینی زغال‌سنگ با توجه به طول و شیب کلیت زغال‌سنگ با رفتار الاستوشکننده

محمدرضا شهبازی[۱]، مهدی نجفی[۱]*، محمد فاتحی مرجی[۱] و ابوالفضل عبداللهی پور[۲]

۱- دانشکده مهندسی معدن و متالورژی، دانشگاه یزد، ایران

۲- دانشکده مهندسی معدن، دانشگاه تهران، ایران

چکیده:

در فرآیند گازکردن زیرزمینی زغال‌سنگ، زغال‌سنگ به صورت برجا به گاز سنتزی تبدیل می‌شود. به منظور افزایش سرعت سوختن زغال‌سنگ در فرآیند UCG، سطح تماس شکست زغال‌سنگ با بخار آب و حرارت باید افزایش یابد. بنابراین باید با افزایش حـرارت و فشـار بخـار آب موجـود در طـول فرآینـد، تعـداد ترک‌هـای ثانویه را افزایش داد. این مقاله بر ساز و کار رشد ترک ثانویه حاصل از ترک‌های از پیش موجود در نمونه‌های زغال‌سنگ تحـت شـرایط بارگـذاری مختلـف تمرکـز دارد. مشخصات هندسی مختلفی از جمله طول ترک‌های از پیش موجود (کلیت‌های زغال‌سنگ) و شیب آن‌ها در نظر گرفتـه شـده اسـت. نتـایج مـدل‌سـازی عـددی نشان داده است که ترک بالهای (که ترک‌های اولیه یا کششی نیز نامیده می‌شوند) به عنوان اولین ترک به دلیل شکسـته شـدن پیونـد کششـی بـین ذره‌هـا در نمونـه گسترش می‌یابد. در نهایت، این ترک‌ها ممکن است منجر به ترکیب و به هم پیوستگی کلیت‌ها شوند. از طرفی ترک های ثانویه یا برشی به صـورت تـرک‌هـای هـم-صفحه و مورب نیز ممکن است در طی فرآیند رشد ترک در نمونه ایجاد شوند. این ترک ها در اثر نیروهای برشی القایی بـین ذرههـا همـراه بـا افـزایش طـول کلیـت اولیه ایجاد شده و ابعاد گسترش آن فراتر از ابعاد بلوک‌های زغال‌سنگ است. بـا رشـد سـریع‌تـر تـرک‌هـای ثانویـه در بلـوک‌هـای زغـال‌سـنگ، سـرعت رشـد فضـای استخراجی افزایش می‌یابد. نتایج حاصل از این تحقیق نشان داده است که که برای دستیابی به شرایط بهینـه، زاویـه مناسـب شـیب کلیـت اولیـه زغـال‌سـنگ بـا رفتـار الاستوشکننده بین ۳۰ تا ۴۵ درجه نسبت به افق است.

کلمات کلیدی: روش UCG، گسترش فضای استخراجی، گسترش ترک، طول و شیب کلیت، مدل پیوند موازی خطی.